ISSN 1070-3284, Russian Journal of Coordination Chemistry, 2016, Vol. 42, No. 11, pp. 719–729. © Pleiades Publishing, Ltd., 2016.
Original Russian Text © O.V. Loseva, T.A. Rodina, A.I. Smolentsev, A.V. Ivanov, 2016, published in Koordinatsionnaya Khimiya, 2016, Vol. 42, No. 11, pp. 683–693.

Syntheses, Supramolecular Structures, and Thermal Behavior of Heteronuclear Gold(III)–Mercury(II) Dithiocarbamatochloride Complexes $[Au\{S_2CN(CH_3)_2\}_2]_2[HgCl_4]$ and $([Au\{S_2CN(C_2H_5)_2\}_2]_2[Hg_2Cl_6] \cdot OC(CH_3)_2)_n$ by ^{13}C MAS NMR, X-ray Diffraction, and Simultaneous Thermal Analysis Data

O. V. Loseva[a], T. A. Rodina[b], A. I. Smolentsev[c, d], and A. V. Ivanov[a, *]

[a] *Institute of Geology and Nature Management, Far Eastern Branch, Russian Academy of Sciences, Blagoveshchensk, 675000 Russia*

[b] *Amur State University, Blagoveshchensk, 675027 Russia*

[c] *Nikolaev Institute of Inorganic Chemistry, Siberian Branch, Russian Academy of Sciences, Novosibirsk, 630090 Russia*

[d] *Novosibirsk State University, Novosibirsk, 630090 Russia*

**e-mail: alexander.v.ivanov@chemist.com*

Received February 22, 2016

Abstract—New heteronuclear gold(III)–mercury(II) compounds are synthesized by the chemisorption reaction of freshly precipitated mercury dimethyl (MeDtc) and diethyl dithiocarbamates (EtDtc) with $[AuCl_4]^-$ anions in a medium of 2 M HCl. The crystals of complexes $[Au\{S_2CN(CH_3)_2\}_2]_2[HgCl_4]$ (**I**) and $([Au\{S_2CN(C_2H_5)_2\}_2]_2[Hg_2Cl_6] \cdot OC(CH_3)_2)_n$ (**II**) are obtained from solutions in methanol and acetone, respectively. The crystal and supramolecular structures of the preparatively isolated compounds are determined by X-ray diffraction analysis (CIF files CCDC nos. 1452118 (**I**) and 1452119 (**II**)). The structure of ionic complex **I** is built of alternating binuclear $[Au_2\{S_2CN(CH_3)_2\}_4]^{2+}$ cations and $[HgCl_4]^{2-}$ anions. A more complicated structure of compound **II** contains centrosymmetric isomeric $[Au\{S_2CN(C_2H_5)_2\}_2]^+$ cations (**A** and **B**) and centrosymmetric binuclear $[Hg_2Cl_6]^{2-}$ anions. The supramolecular structure of compound **II** is formed due to pairs of Au···S secondary bonds between the adjacent gold(III) complex cations resulting in the formation of linear polymeric chains $[\cdots\mathbf{A}\cdots\mathbf{B}\cdots]_n$ (directed along the *x* crystallographic axis). Isomeric cations **A** and **B** are alternated along the chains. The character of thermolysis of the complexes is studied and the regeneration conditions of bound gold are revealed by the simultaneous thermal analysis data. The thermal destruction of compounds **I** and **II** occurs simultaneously at the cationic and anionic moieties of the compounds to reduce gold(III) accompanied by the release and subsequent sublimation of mercury(II) chloride. The final product of the thermal transformations of the complexes is reduced elemental gold.

Keywords: chemisorption binding of gold(III) from solution, mercury(II) dialkyldithiocarbamates, heteronuclear gold(III)-mercury(II) complexes, supramolecular self-organization, secondary interactions

DOI: 10.1134/S1070328416110063

INTRODUCTION

Dialkyl dithiocarbamate complexes of transition metals are used in various areas of chemistry and chemical technology, agriculture, and medicine [1–8]. They are promising precursors for the preparation of film and nanosized metal sulfides and heteropolymetallic sulfides with the semiconducting and luminescence properties [1–4]. The complexes bearing dithiocarbamate ligands exhibit anticancer [5, 6] and antibacterial [7, 8] activities. In addition, transition metal dithiocarbamates are capable of efficient chemisorption binding of gold(III) from solutions to form complicatedly organized in the structural respect heterometallic dithiocarbamatochloride complexes, which are interesting for coordination and experimental chemistry. We have previously obtained a whole series of heterometallic complexes of the ionic type including along with gold(III) zinc [9–11], cadmium [12–14], bismuth(III) [15, 16], thallium(I) [17, 18], and iron(III) [19]. The structures and properties of the synthesized compounds were established by the X-ray diffraction, MAS NMR (^{13}C, ^{15}N, and ^{113}Cd), and

simultaneous thermal analysis (STA) data. Continuing the studies on the chemisorption binding of gold(III) by dithiocarbamates (Dtc) of metals of the zinc subgroup, it seemed interesting to prepare new gold(III)–mercury(II) heteropolynuclear complexes as individual forms of Au^{3+} binding from solutions of mercury(II) dialkyl dithiocarbamates.

New heterometallic gold(III)–mercury(II) dialkyl dithiocarbamatochloride complexes, $[Au_2\{S_2CN(CH_3)_2\}_4][HgCl_4]$ (**I**) and $([Au\{S_2CN(C_2H_5)_2\}_2]_2[Hg_2Cl_6] \cdot OC(CH_3)_2)_n$ (**II**), were synthesized in this work. The structures of the obtained compounds were solved by X-ray diffraction analysis, and the thermal behavior was studied on the STA data.

EXPERIMENTAL

The starting mercury complexes $[Hg\{S_2CN(CH_3)_2\}_2]$ [20] and $[Hg_2\{S_2CN(C_2H_5)_2\}_4]$ [21] were obtained by the precipitation of Hg^{2+} cations from the aqueous phase with solutions of $Na\{S_2CN(CH_3)_2\} \cdot xH_2O$ (Aldrich) and $Na\{S_2CN(C_2H_5)_2\} \cdot 3H_2O$ (Sigma–Aldrich), respectively, taken in stoichiometric ratios. The individual states of all compounds were confirmed by the following data of ^{13}C CP/MAS NMR spectroscopy (δ, ppm):

$Na\{S_2CN(CH_3)_2\} \cdot xH_2O$: 209.7 (51)*, 207.4 (43)* ($-S_2CN=$); 47.5 (39)*, 47.0 (31)* ($-CH_3$).

$[Hg\{S_2CN(CH_3)_2\}_2]$: 201.9 (48)* ($-S_2CN=$); 49.5 (35)* ($-CH_3$).

$Na\{S_2CN(C_2H_5)_2\} \cdot 3H_2O$ (1 : 2 : 2): 206.5 (51)* ($-S_2CN=$); 48.6 (71)* ($=NCH_2-$); 13.2 ($-CH_3$).

$[Hg_2\{S_2CN(C_2H_5)_2\}_4]$: 204.0 (42)*, 201.1 (39)* (1 : 1, $-S_2CN=$); 53.5, 52.3 (1 : 1, $=NCH_2-$); 14.1, 12.7 (1 : 3, $-CH_3$).

(*Asymmetric $^{13}C-^{14}N$ doublets [22, 23], in Hz).

Syntheses of compounds I and II. Tetrakis(*N,N*-dimethyldithiocarbamato-*S,S'*)digold(III) tetrachloromercurate(II) (**I**) and polymeric bis(*N,N*-diethyldithiocarbamato-*S,S'*)gold(III) hexachlorodimercurate(II) (**II**) were synthesized by the reactions of freshly precipitated mercury(II) dimethyl (MeDtc) and diethyl (EtDtc) dithiocarbamates with solutions of $AuCl_3$ in 2 M HCl. A solution (10 mL) of $AuCl_3$ (in 2 M HCl) containing gold (44 or 39 mg) was poured to mercury(II) MeDtc/EtDtc (100 mg), and the mixture was stirred for 15 min. The residual content of gold in the solution was determined on an atomic absorption spectrometer (class 1, Hitachi, model 180–50). The obtained yellow precipitates were filtered off, washed with water, and dried on the filter. The yields were 95 and 92%, respectively. Gold(III) binding from solutions can be presented by the following heterogeneous reactions:

$$2[Hg\{S_2CN(CH_3)_2\}_2] + 2H[AuCl_4] = [Au_2\{S_2CN(CH_3)_2\}_4][HgCl_4] + HgCl_2 + 2HCl,$$

$$[Hg_2\{S_2CN(C_2H_5)_2\}_4] + 2H[AuCl_4] = [Au\{S_2CN(C_2H_5)_2\}_2]_2[Hg_2Cl_6] + 2HCl.$$

It is important that gold(III) binding is not accompanied, in the second case, by the partial escape of mercury(II) to the solution and is formally reduced to the addition of two $AuCl_3$ molecules to the binuclear molecule of the complex-chemisorbent.

The crystals for X-ray diffraction analysis were obtained by the dissolution of the precipitates in methanol (**I**) or acetone (**II**) followed by the slow evaporation of the solvents. Crystallization gave yellow transparent prismatic crystals of compounds **I** and **II**.

Elemental analyses to C, H, and N for compounds **I** and **II** were carried out on a Euro EA-3000 automated elemental analyzer.

For $C_{12}H_{24}N_4S_8Cl_4Au_2Hg$ (**I**)			
anal. calcd., %:	C, 11.84;	H, 1.99;	N, 4.60.
Found, %:	C, 11.9;	H, 2.0;	N, 4.6.
For $C_{23}H_{46}ON_4S_8Cl_6Au_2Hg_2$ (**II**)			
anal. calcd., %:	C, 16.65;	H, 2.79;	N, 3.38.
Found, %:	C, 16.2;	H, 2.6;	N, 3.4.

Compound **II** was also characterized by the data of ^{13}C MAS NMR spectroscopy (δ, ppm): 196.4, 194.4 (1 : 1, $-S_2CN=$); 52.5, 50.5, 49.3, 48.1, 45.4 ($-CH_2-$); 16.2, 15.5, 15.1, 13.8 ($-CH_3$); 206.9 (=CO), 34.5 ($-CH_3$, $OC(CH_3)_2$).

(We failed to obtain the ^{13}C MAS NMR spectrum of satisfactory quality for compound **I**.)

^{13}C MAS NMR spectra were recorded on a CMX-360 spectrometer (Agilent/Varian/Chemagnetics InfinityPlus) with a working frequency of 90.52 MHz, a superconducting magnet (B_0 = 8.46 T), and Fourier transformation. Proton cross polarization was used, and the decoupling effect was applied to suppress $^{13}C-^{1}H$ interactions using the radiofrequency field at the resonance field of protons [24]. A sample of compound **II** (~40 mg) was placed in a 4.0-mm ZrO_2 ceramic rotor. When measuring ^{13}C MAS NMR spectra, rotation at the magic angle at frequencies of 10100–10700(1) Hz was used (scan number 3800–5400, duration of proton π/2 pulses 5.0 μs, $^{1}H-^{13}C$ contact time 2.0 ms, interval between pulses 2.0 s). The isotropic chemical shifts (δ) of the ^{13}C nuclei (ppm) are given relative to one of the components of crystalline adamantane used as an external standard (δ = 38.48 ppm relative to tetramethylsilane).

X-ray diffraction analyses were carried out from single crystals of compounds **I** and **II** on a Bruker-Nonius X8 Apex CCD diffractometer (MoK_α radiation, λ = 0.71073 Å, graphite monochromator) at

Table 1. Crystallographic data and experimental and refinement parameters for the structures of compounds **I** and **II**

Parameter	Value	
	Compound **I**	Compound **II**
FW	1217.16	1658.93
Crystal system	Monoclinic	Triclinic
Space group	$C2/c$	$P\overline{1}$
a, Å	15.8238(4)	9.3664(2)
b, Å	10.2824(3)	10.3762(2)
c, Å	18.7160(7)	12.5463(3)
α, deg	90	72.2940(10)
β, deg	107.8750(10)	72.5590(10)
γ, deg	90	81.1380(10)
V, Å^3	2898.22(16)	1105.52(4)
Z	4	1
ρ_{calcd}, g/cm^3	2.789	2.492
μ, mm^{-1}	16.341	14.303
F(000)	2232	768
Crystal size, mm	0.15 × 0.07 × 0.05	0.25 × 0.15 × 0.07
θ Range, deg	4.04–27.52	4.02–27.50
Ranges of reflection indices	$-17 \leqslant h \leqslant 20$, $-13 \leqslant k \leqslant 13$, $-24 \leqslant l \leqslant 19$	$-7 \leqslant h \leqslant 12$, $-13 \leqslant k \leqslant 13$, $-15 \leqslant l \leqslant 16$
Measured reflections	11153	11089
Independent reflections (R_{int})	3318 (0.0285)	5001 (0.0323)
Reflections with $I > 2\sigma(I)$	2870	4409
Refinement parameters	145	235
GOOF	1.013	0.978
R factors for $F^2 > 2\sigma(F^2)$	$R_1 = 0.0201$, $wR_2 = 0.0432$	$R_1 = 0.0259$, $wR_2 = 0.0481$
R factors for all reflections	$R_1 = 0.0267$, $wR_2 = 0.0447$	$R_1 = 0.0316$, $wR_2 = 0.0497$
$\Delta\rho_{max}/\Delta\rho_{min}$, e/Å^3	−0.558/1.191	−1.056/0.955

296(2) and 150(2) K, respectively. Data collection was performed using a standard procedure: φ and ω scan modes of narrow (0.5°) frames. An absorption correction was applied empirically using the SADABS program [25]. The structures were determined by a direct method and refined by least squares (on F^2) in the full-matrix anisotropic approximation of non-hydrogen atoms. The positions of the hydrogen atoms were calculated geometrically and included into the refinement in the riding model. The solvate molecule of acetone in compound **II** is disordered between two equivalent positions with equal populations.

Data were collected and edited and the unit cell parameters were refined using the APEX2 [25] and SAINT programs [25]. The calculations on structure determination and refinement were performed using the SHELXTL program package [25]. The main crystallographic data and refinement results for the structures of compounds **I** and **II** are presented in Table 1. Selected bond lengths and angles are given in Table 2.

The coordinates of atoms, bond lengths, and bond angles were deposited with the Cambridge Crystallographic Data Centre (CIF files CCDC nos. 1452118 (**I**) and 1452119 (**II**); deposit@ccdc.cam.ac.uk or http://www.ccdc.cam.ac.uk).

The thermal behavior of compounds **I** and **II** were studied by the STA method with simultaneous recording thermogravimetry (TG) and differential scanning calorimetry (DSC) curves. The study was carried out on a STA 449C Jupiter instrument (NETZSCH) in corundum crucibles under a cap with a hole providing a vapor pressure of 1 atm during the thermal decomposition of the sample. The heating rate was 5°C/min to 1100°C in an argon atmosphere. The samples were

Table 2. Selected bond lengths (*d*) and bond (ω) and torsion (φ) angles in the structures of compounds **I** and **II***

Compound **I**			
Bond	*d*, Å	Bond	*d*, Å
Au(1)–S(1)	2.3288(10)	N(1)–C(1)	1.304(5)
Au(1)–S(2)	2.3481(11)	N(1)–C(2)	1.478(5)
Au(1)–S(3)	2.3343(10)	N(1)–C(3)	1.461(5)
Au(1)–S(4)	2.3433(10)	N(2)–C(4)	1.299(5)
Au(1)···S(2)[a]	3.4247(10)	N(2)–C(5)	1.449(5)
S(1)–C(1)	1.717(4)	N(2)–C(6)	1.463(5)
S(2)–C(1)	1.734(4)		
S(3)–C(4)	1.736(4)	Hg(1)–Cl(1)	2.5456(10)
S(4)–C(4)	1.732(4)	Hg(1)–Cl(2)	2.4596(11)
Angle	ω, deg	Angle	ω, deg
S(1)Au(1)S(2)	75.39(4)	Au(1)S(4)C(4)	86.13(13)
S(1)Au(1)S(3)	102.99(4)	S(1)C(1)S(2)	111.9(2)
S(1)Au(1)S(4)	177.58(4)	S(3)C(4)S(4)	111.7(2)
S(2)Au(1)S(3)	175.82(4)		
S(2)Au(1)S(4)	105.76(4)	Cl(1)Hg(1)Cl(2)	105.25(4)
S(3)Au(1)S(4)	75.72(3)	Cl(1)Hg(1)Cl(1)[b]	108.37(5)
Au(1)S(1)C(1)	86.81(13)	Cl(1)Hg(1)Cl(2)[b]	108.71(4)
Au(1)S(2)C(1)	85.83(14)	Cl(2)Hg(1)Cl(2)[b]	120.15(6)
Au(1)S(3)C(4)	86.31(14)		
Angle	φ, deg	Angle	φ, deg
Au(1)S(1)S(2)C(1)	178.2(2)	S(2)C(1)N(1)C(2)	−178.9(3)
Au(1)S(3)S(4)C(4)	−176.5(2)	S(2)C(1)N(1)C(3)	2.0(5)
S(1)Au(1)C(1)S(2)	178.4(2)	S(3)C(4)N(2)C(5)	1.1(5)
S(3)Au(1)C(4)S(4)	−176.9(2)	S(3)C(4)N(2)C(6)	−175.0(3)
S(1)C(1)N(1)C(2)	0.1(5)	S(4)C(4)N(2)C(5)	−179.6(3)
S(1)C(1)N(1)C(3)	−178.9(3)	S(4)C(4)N(2)C(6)	4.3(5)
Compound **II**			
Bond	*d*, Å	Bond	*d*, Å
Cation **A**		Cation **B**	
Au(1)–S(1)	2.3349(11)	Au(2)–S(3)	2.3257(11)
Au(1)–S(2)	2.3406(10)	Au(2)–S(4)	2.3418(10)
Au(1)···S(3)[b]	3.8794(11)	Au(2)···S(2)	3.5421(11)
S(1)–C(1)	1.733(4)	S(3)–C(6)	1.729(4)
S(2)–C(1)	1.727(4)	S(4)–C(6)	1.728(4)
N(1)–C(1)	1.301(5)	N(2)–C(6)	1.302(5)
N(1)–C(2)	1.488(6)	N(2)–C(7)	1.475(5)
N(1)–C(4)	1.477(5)	N(2)–C(9)	1.478(5)
C(2)–C(3)	1.511(7)	C(7)–C(8)	1.513(7)
C(4)–C(5)	1.487(7)	C(9)–C(10)	1.516(6)
Anion			
Hg(1)–Cl(1)	2.5671(12)	Hg(1)–Cl(3)	2.4157(11)
Hg(1)–Cl(2)	2.4045(11)	Hg(1)–Cl(1)[c]	2.6896(11)

Table 2. (Contd.)

Compound **II**			
Angle	ω, deg	Angle	ω, deg
Cation **A**		Cation **B**	
S(1)Au(1)S(2)	75.27(4)	S(3)Au(2)S(4)	75.30(4)
S(1)Au(1)S(2)[a]	104.73(4)	S(3)Au(2)S(4)[b]	104.70(4)
Au(1)S(1)C(1)	86.78(14)	Au(2)S(3)C(6)	87.1(2)
Au(1)S(2)C(1)	86.75(14)	Au(2)S(4)C(6)	86.56(14)
S(1)C(1)S(2)	111.2(2)	S(3)C(6)S(4)	111.1(2)
Anion			
Cl(1)Hg(1)Cl(2)	115.69(4)	Cl(2)Hg(1)Cl(1)[c]	110.03(4)
Cl(1)Hg(1)Cl(3)	110.31(4)	Cl(3)Hg(1)Cl(1)[c]	105.09(4)
Cl(1)Hg(1)Cl(1)[c]	87.58(3)	Hg(1)Cl(1)Hg(1)[c]	92.43(3)
Cl(2)Hg(1)Cl(3)	122.04(4)		
Angle	φ, deg	Angle	φ, deg
Cation **A**		Cation **B**	
Au(1)S(1)S(2)C(1)	178.5(2)	Au(2)S(3)S(4)C(6)	179.8(3)
S(1)Au(1)C(1)S(2)	178.7(2)	S(3)Au(2)C(6)S(4)	179.8(2)
S(1)C(1)N(1)C(2)	−1.5(6)	S(3)C(6)N(2)C(7)	1.8(6)
S(1)C(1)N(1)C(4)	179.8(3)	S(3)C(6)N(2)C(9)	−177.1(3)
S(2)C(1)N(1)C(2)	178.9(3)	S(4)C(6)N(2)C(7)	−179.8(3)
S(2)C(1)N(1)C(4)	0.3(6)	S(4)C(6)N(2)C(9)	1.3(6)

* Symmetry transformations: [a] $1/2 - x, 1/2 - y, 1 - z$; [b] $-x, y, 1/2 - z$ (**I**); [a] $-x - 1, 1 - y, 1 - z$; [b] $-x, 1 - y, 1 - z$; [c] $-x, 1 - y, -z$ (**II**).

additionally recorded in aluminum crucibles to reveal more distinctly thermal effects in the low-temperature region. The weight of the samples was 1.726–3.003 (**I**) and 2.073–8.043 mg (**II**). The accuracy of temperature measurements was ±0.8°C, and that of a mass change was $\pm 1 \times 10^{-4}$ mg. When recording the TG and DSC curves, the correction file and calibrations by temperature and sensitivity for specified temperature program and heating rate were used. The melting points of the complexes were independently determined on a PTP(M) instrument (OAO Khimlaborpribor).

Electron scanning microscopy and electron-probe X-ray microanalysis. The studies were carried out at the Analytical Center of the Institute of Geology and Nature Management (Far East Branch, Russian Academy of Sciences). The dispersion and morphological features of the samples were determined by high-resolution scanning electron microscopy on a JSM-35C JEOL analytical scanning electron microscope equipped with a 35-SDS spectrometer with wave dispersion. The secondary electron image was used (morphology and microstructure). The qualitative determination of elements was carried out by electron-probe X-ray microanalysis on a RONTEC energy dispersive spectrometer integrated with a LEO-1420 scanning electron microscope.

RESULTS AND DISCUSSION

The starting mercury MeDtc and EtDtc complexes are finely crystalline lemon-colored and pale yellow precipitates, respectively. According to the electron-probe X-ray microanalysis data, their qualitative compositions are shown by the Hg, C, N, and S spectral lines (Figs. 1a, 1a'). The contact of mercury(II) Dtcs with solutions of $AuCl_3$ in 2 M HCl leads to the reformation of the precipitates with color deepening to golden-yellow and the simultaneous decoloration of the working solutions. The chemisorption interaction is rather fast, and the degree of binding of gold(III) from solutions achieves 99.5 (**I**) and 98.2% (**II**) already in 15 min. The changes observed indicate the formation of new compounds in the systems studied. The energy dispersive spectra of the formed compounds **I** and **II** contain additional signals due to the presence of gold and chlorine in the samples studied (Figs. 1b, 1b').

The ^{13}C MAS NMR spectrum of crystalline complex **II** (Fig. 2) exhibits resonance signals of the

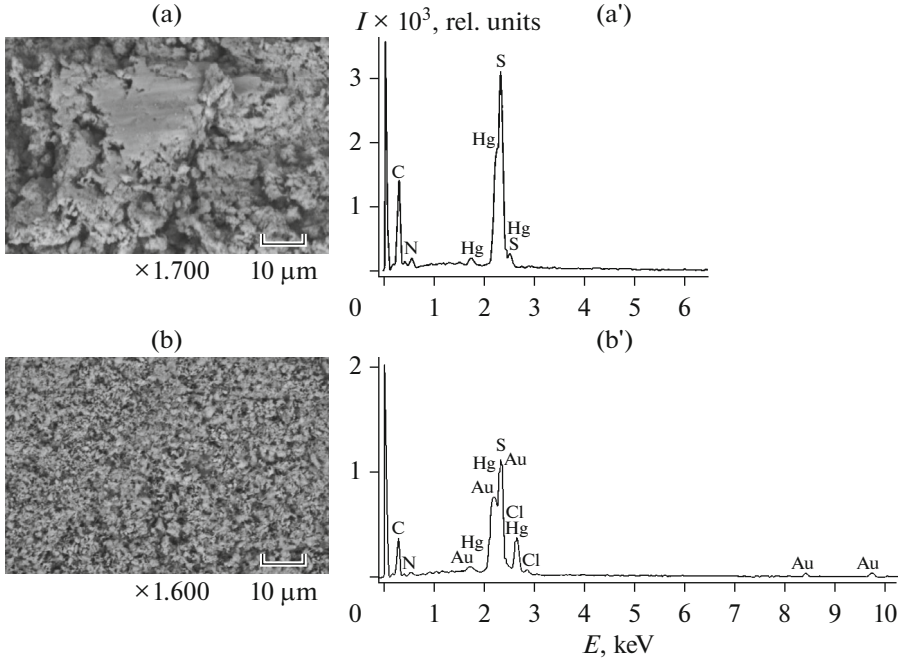

Fig. 1. (a, b) Size and shape of particles and (a', b') the energy dispersive spectra for complexes (a, a') $[Hg\{S_2CN(CH_3)_2\}_2]$ and (b, b') $[Au\{S_2CN(CH_3)_2\}_2]_2[HgCl_4]$.

=NC(S)S–, $-CH_2-$, and $-CH_3$ groups of the Dtc ligands and the =CO and $-CH_3$ groups of the outer-sphere acetone molecule ((see Section '**Syntheses of compounds I and II**'). As compared to the starting mercury(II) EtDtc complex, the $\delta(^{13}C)$ chemical shifts of the dithiocarbamate groups in complex **II** are characterized by substantially lower values because of the redistribution of the Dtc ligands over the internal coordination sphere of gold, whose electron system can participate more efficiently in the additional shielding of the carbon nuclei of the =NC(S)S– groups. Two (1 : 1) resonance signals of the ^{13}C =NC(S)S– groups indicate that the structure of complex **II** contains two structurally nonequivalent ligands. The crystal and supramolecular structures of compounds **I** and **II** were resolved by X-ray diffraction analysis in order to establish the structural organization of the complexes.

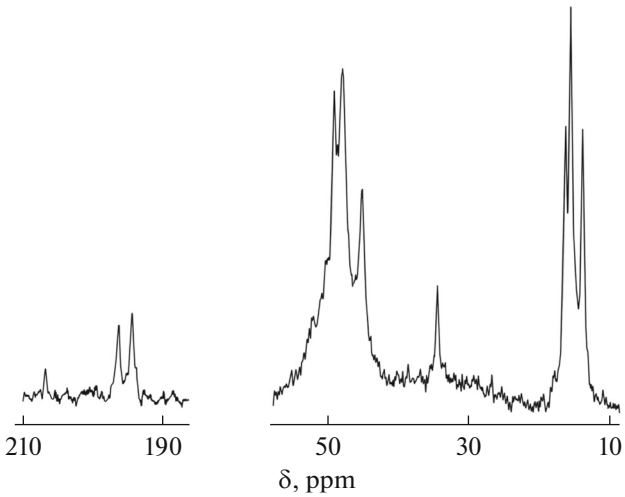

Fig. 2. ^{13}C MAS NMR spectrum of compound **II**. Scan number/rotation frequency of the sample was 5400/10.1 kHz.

The unit cells of compounds **I** and **II** include 4 and 1 formula units (Figs. 3, 4). The cationic moiety of compound **I** is presented by the $[Au\{S_2CN(CH_3)_2\}_2]^+$ noncentrosymmetric complex ion. The structure of compound **II** includes two isomeric centrosymmetric $[Au\{S_2CN(C_2H_5)_2\}_2]^+$ cations: cation **A** with the Au(1) atom and cation **B** with Au(2) (Table 2), which is completely consistent with the NMR data. In each complex cation, the gold atom coordinates two Dtc ligands through the S,S'-bidentate mode to form the tetragonal $[AuS_4]$ chromophore with the low-spin inner-orbital dsp^2-hybrid state of the gold atom. The anionic moiety of the complexes is presented by the distorted tetrahedral $[HgCl_4]^{2-}$ (**I**) and centrosymmetric $[Hg_2Cl_6]^{2-}$ (**II**) anions (Figs. 5b, 6b). In each complex anion, the metal atom (sp^3-hybrid state) is surrounded by four chlorine atoms. The ClHgCl bond angles lying in the ranges 105.25°–120.15° (**I**) and 87.58°–122.04° (**II**) (Table 2) considerably deviate from the purely tetrahedral value, which is typical of halogenomercurate(II) ions [26, 27]. The Hg–Cl bonds in the

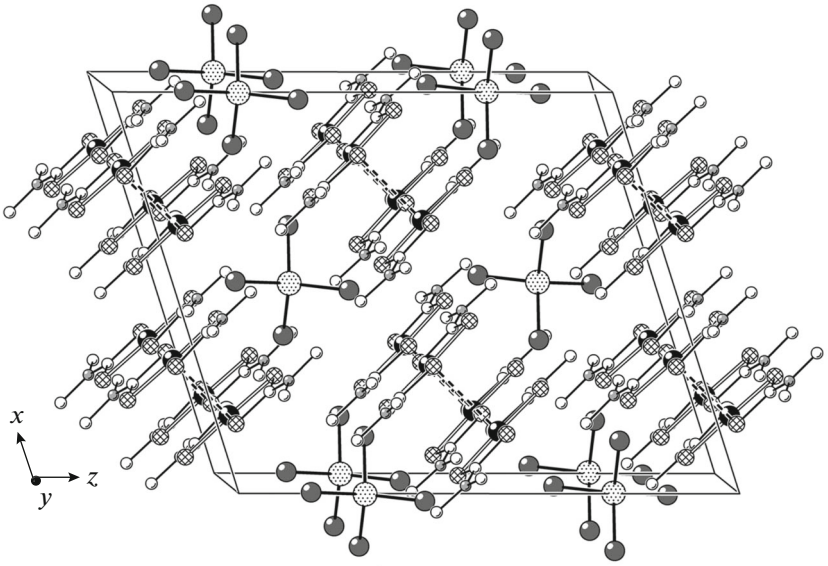

Fig. 3. Projection of the structure of compound **I** on the *xz* plane.

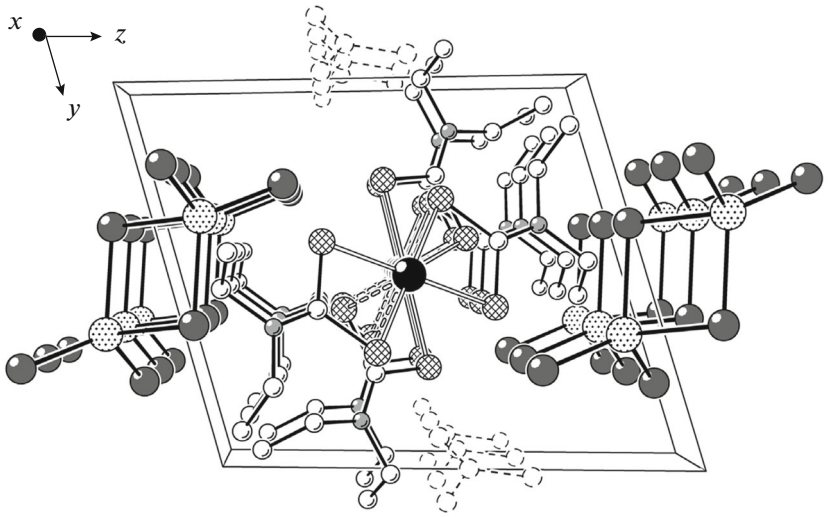

Fig. 4. Projection of the structure of compound **II** on the *yz* plane.

$[HgCl_4]^{2-}$ ion are nonequivalent in pairs. In the binuclear anion, the bonds of the cadmium atom with the terminal chlorine atoms are noticeably stronger (2.4045 and 2.4157 Å) than those with the bridging atoms (2.5671 and 2.6896 Å).

In each of two complexes, the gold atom coordinates two Dtc ligands nearly through the isobidentate mode: the Au–S bond length lies in a narrow range of 2.3257–2.3481 Å. This coordination mode is accompanied by the formation of small four-membered metallocycles $[AuS_2C]$ with the distances Au···C 2.815–2.829 Å and S···S 2.851–2.871 Å, which are significantly shorter than the sums of the van der Waals radii of the corresponding pairs of atoms: 3.36 and 3.60 Å [28–30]. The atoms in the $[AuS_2C]$ groups are nearly coplanar: the AuSSC and SAuCS torsion angles slightly (by 0.2°–3.5°) deviate from 180° or 0° (Table 2).

The $C_2NC(S)S$ groups in the Dtc ligands are also planar, which is indicated by the SCNC torsion angles, whose values are close to 180° or 0° (Table 2). The only significant deviation from the plane is demonstrated by the C(6) atom in compound **I**: the torsion angles are S(3)C(4)N(2)C(6) –175.0° and S(4)C(4)N(2)C(6) 4.3°. The strength of the N–C(S)S bonds (1.299–1.304 Å) is much higher than that of

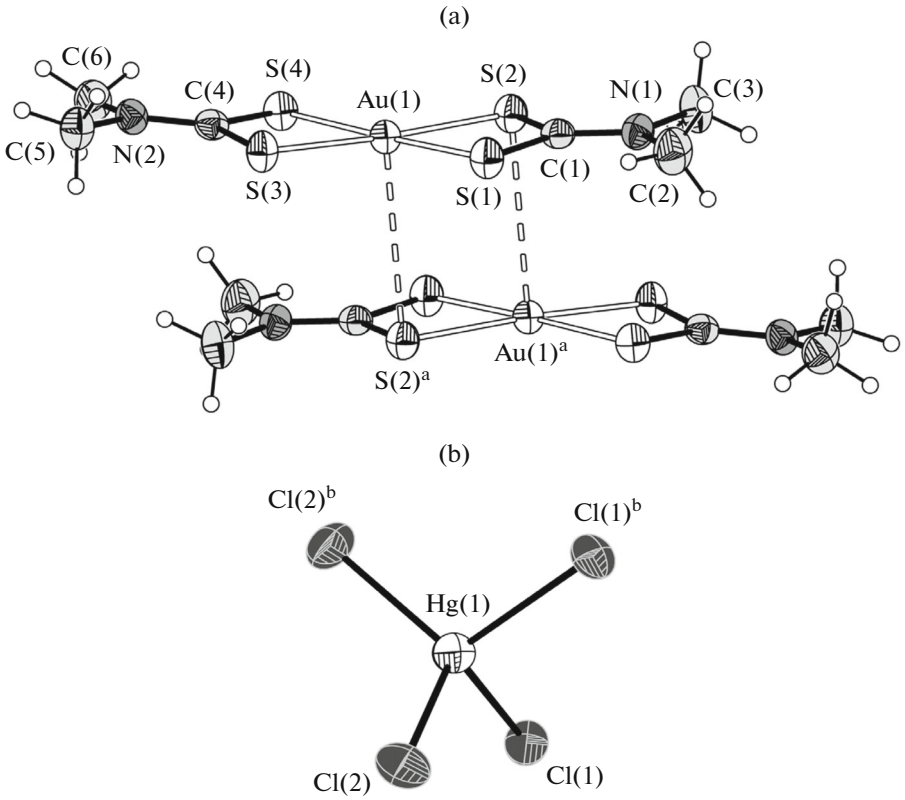

Fig. 5. Structures of the (a) $[Au_2\{S_2CN(CH_3)_2\}_4]^{2+}$ binuclear complex cation and (b) $[HgCl_4]^{2-}$ anion of compound **I**. Ellipsoids of 50% probability; the Au···S secondary bonds are shown by dash.

N–CH_2 (1.449–1.488 Å) because of the contribution of double bonding to the formally ordinary bond and the admixing of sp^2 to the sp^3-hybrid state of the nitrogen and carbon atoms due to the mesomeric effect.

The organization of the structures of compounds **I** and **II** differs substantially. The gold(III) complex cations in compound **I** are unified by pairs of the secondary[1] Au···S bonds to form centrosymmetric dimers $[Au_2\{S_2CN(CH_3)_2\}_4]^{2+}$ with the antiparallel orientation of the mononuclear fragment and an Au···Au distance of 4.247 Å (Fig. 5a). In each cation, only one sulfur atom, S(2) of one of the MeDtc ligands, participates in secondary interactions. The lengths of the paired secondary bonds Au(1)···S(2)^a and Au(1)^a···S(2) (3.4247 Å) are somewhat shorter than the sum of the van der Waals radii of the gold and sulfur atoms (3.46 Å) [28–30]. In the crystal structure of compound **I**, the gold(III) binuclear cations discussed alternate with the $[HgCl_4]^{2-}$ discrete anions forming piles oriented along the *y* crystallographic axis (Fig. 3).

Complex **II** demonstrates a more complicated character of the structure. Two isomeric cations, **A** and **B**, are involved in its supramolecular self-organization. Each of the cations forms two pairs of nonequivalent secondary Au···S bonds with two adjacent cations due to the gold atom and two diagonally arranged sulfur atoms: Au(1)···S(3)^b and Au(1)···S(3)^c 3.8794, Au(2)···S(2) and Au(2)···S(2)^b 3.5421 Å. This interaction leads to the formation of linear polymeric chains $[\cdots\mathbf{A}\cdots\mathbf{B}\cdots]_n$ (angle Au(1)Au(2)Au(1)^d 180°) oriented along *x* crystallographic axis, and isomeric cations **A** and **B** are alternated along the chains (Fig. 6a). The strength of binding between the adjacent cations in the chain discussed is lower than that in the $[Au_2\{S_2CN(CH_3)_2\}_4]^{2+}$ binuclear cation, resulting in an expected elongation of the Au(1)···Au(2) distance (to 4.683 Å).

The thermal behavior of compounds **I** and **II** was studied by the STA method in an argon atmosphere with the simultaneous detection of the TG and DSC curves. The complexes show different characters of thermal destruction (Figs. 7, 8). The thermolysis of compound **I** formally proceeds in one stage in a range of ~215–365°C (Fig. 7*a*). The main mass loss (64.70% of the initial value) falls onto the steeply descending region of the TG curve, indicating that the thermolysis proceeds simultaneously at the cation and anion. The subsequent flat region (~365–800°C) shows the

[1] The concept of secondary bonds was proposed [31] for the description of interactions characterized by the distances comparable with the sums of the van der Waals radii of the corresponding atoms.

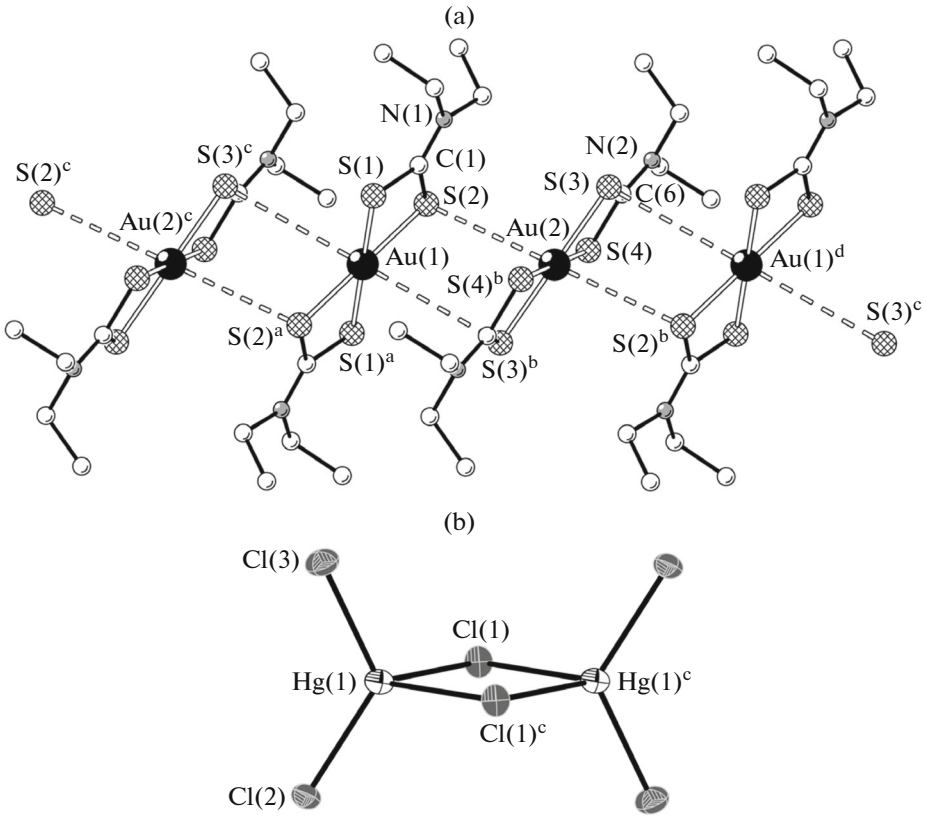

Fig. 6. (a) Fragment of the $([Au\{S_2CN(C_2H_5)_2\}_2]^+)_n$ polynuclear chain in complex **II** and (b) the structure of the $[Hg_2Cl_6]^{2-}$ binuclear cation. Ellipsoids of 50% probability; the Au···S secondary bonds are shown by dash.

desorption of volatile thermolysis products. The residual mass at 1100°C is 32.25%, which is consistent with the calculated value (32.36%) for reduced gold. Gold balls 60–340 μm in size without visible slag traces were observed on the crucible bottom after the end of the process (Fig. 7*c*). The intense endotherm in the low-temperature region of the DSC curve (Fig. 7*b*) is due to the melting of the complex with decomposition (the extrapolated temperature of the process is 281.9°C). It was found by the independent determination of mp in a glass capillary that the melting of the complexes in a range of 274–276°C was accompanied by vigorous gas evolution. The high-temperature region of the DSC curve exhibits an endotherm showing the melting of reduced gold (extrapolated mp = 1062.9°C).

The TG curve detects several stages of mass loss and indicates a more complicated character of the thermal destruction of complex **II** (Fig. 8*a*). The mass loss in the first (low-temperature) region (~107–136°C) is 3.52%, which is consistent with the calculated value (3.50%) for a solvate acetone molecule. The desolvation of compound **II** is shown in the DSC curve by the endotherm with an extreme at 113.6°C (Fig. 8*b*). Then, when the mass of the sample was stabilized, the DSC curve detected the next endotherm with an extreme at 171.8°C assigned to the melting of the non-solvated form of the complex (extrapolated m.p. = 169.9°C). The melting of complex **II** was independently established in a range of 168–170.0°C.

The region of the TG curve from 187 to 455°C detects the main mass loss (68.59%), which substantially exceeds the calculated value for the "dithiocarbamate" moiety of compound **II** (35.75%). This indicates the thermolysis of the complex simultaneously at the cationic and anionic moieties: with the reduction of gold(III) to the metal and the release and subsequent evaporation of $HgCl_2$. Several inflection points in the TG curve indicate a complicated character of the occurred processes. The DSC curve in the discussed region is presented by a broadened asymmetric thermal effect. The complicated internal structure of the latter revealed by differentiation is caused by the superposition of the exo- and endotherms with extremes at 247.7 and 284.6°C, respectively (Fig. 8*b*). The exotherm is most pronounced when recording in an aluminum crucible (Fig. 8*c*). The problem of $HgCl_2$ evaporation required a more detailed consideration. The matter is that 32.73% of the total weight of complex **II** fall onto the fraction of formed mercury(II) chloride. However, it follows from an analysis of the TG curve that the residual mass is only 13.15% (except for reduced gold) when the boiling point of

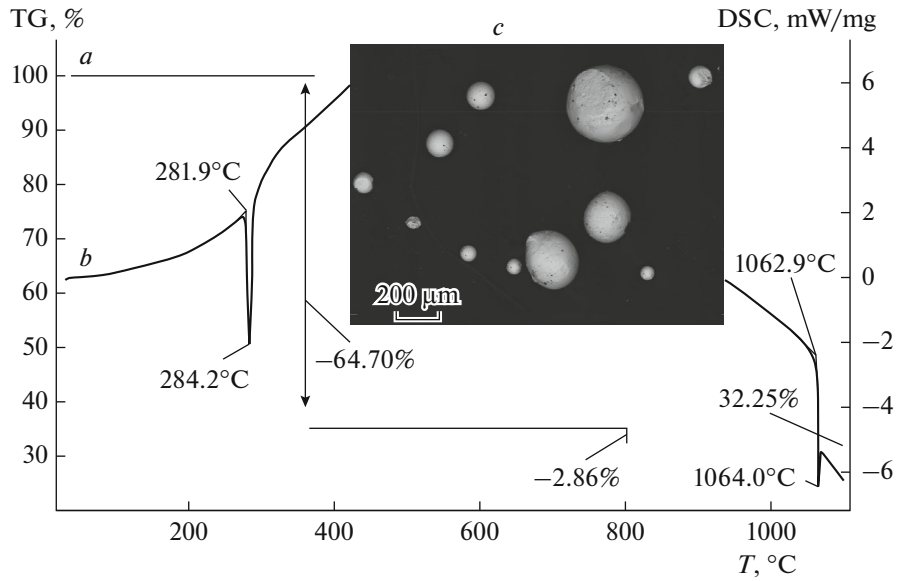

Fig. 7. (*a*) TG and (*b*) DSC curves for complex **I**; (*c*) balls of reduced gold after the completion of the process.

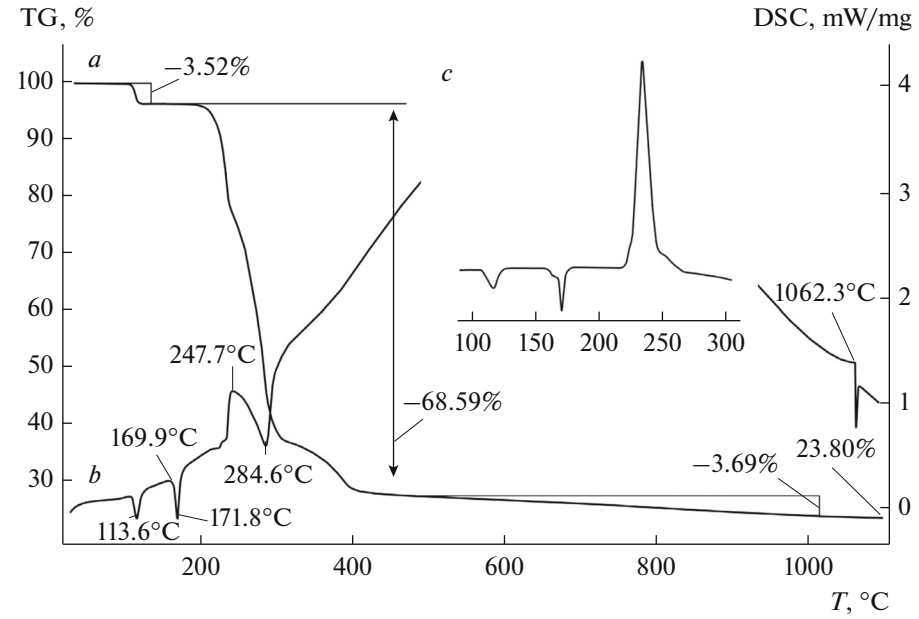

Fig. 8. (*a*) TG and (*b*) DSC curves for complex **II**; (*c*) the low-temperature DSC region detected in an aluminum crucible.

$HgCl_2$ is achieved (301.8°C [32]). Therefore, the thermal behavior of compact $HgCl_2$ (11.415 mg) was studied to check the possibility of the quantitative evaporation of mercury(II) chloride far from its bp. It was found that the first indications to sublimation were observed already at 170°C and the sublimation was completed to 270°C when the mp of $HgCl_2$ even was not achieved (280.0°C [32]).

The final, third stage (~455–1020°C) with a mass loss of 3.69% is caused by the final desorption of volatile thermolysis products of complex **II**. The residual mass at 1100°C (23.80%) only insignificantly exceeds the value calculated for reduced gold (23.75%). Thus, the final thermolysis product for compounds **I** and **II** is metallic gold (the DSC curve detects the endotherm of its melting, and the extrapolated mp is 1062.3°C),

which is quantitatively regenerated under relatively mild conditions.

ACKNOWLEDGMENTS

The authors are grateful to O.N. Antzutkin (Luleå University of Technology, Sweden) for the kindly presented possibility of recording ^{13}C MAS NMR spectra.

This work was supported in part by the Presidium of the Far East Branch of the Russian Academy of Sciences (project no. 15–I–3–001) and the Ministry of Education and Science of the Russian Federation (project no. 1452.2014/9).

REFERENCES

1. Srinivasan, N., Thirumaran, S., and Ciattini, S., *J. Mol. Struct.*, 2014, vol. 1076, p. 382.
2. Sivagurunathan, G.S., Ramalingam, K., and Rizzoli, C., *Polyhedron*, 2013, vol. 65, p. 316.
3. Ajibade, P.A., Onwudiwe, D.C., and Moloto, M.J., *Polyhedron*, 2011, vol. 30, no. 2, p. 246.
4. Chesman, A.S.R., van Embden, J., Duffy, N.W., et al., *Cryst. Growth Design*, 2013, vol. 13, p. 1712.
5. Hogarth, G., *Mini-Rev. Med. Chem.*, 2012, vol. 12, no. 12, p. 1202.
6. Nardon, C., Boscutti, G., and Fregona, D., *Anticancer Res.*, 2014, vol. 34, no. 1, p. 487.
7. Ferreira, I.P., De Lima, G.M., Paniago, E.B., et al., *Eur. J. Med. Chem.*, 2012, vol. 58, p. 493.
8. Mamba, S.M., Mishra, A.K., Mamba, B.B., et al., *Spectrochim. Acta, Part A*, 2010, vol. 77, p. 579.
9. Ivanov, A.V., Loseva, O.V., Rodina, T.A., et al., *Russ. J. Inorg. Chem.*, 2014, vol. 59, no. 8, p. 807.
10. Loseva, O.V. and Ivanov, A.V., *Russ. J. Inorg. Chem.*, 2014, vol. 59, no. 12, p. 1491.
11. Loseva, O.V., Rodina, T.A., and Ivanov, A.V., *Russ. J. Coord. Chem.*, 2013, vol. 39, no. 6, p. 463.
12. Rodina, T.A., Ivanov, A.V., Gerasimenko, A.V., et al., *Polyhedron*, 2012, vol. 40, no. 1, p. 53.
13. Loseva, O.V., Rodina, T.A., Ivanov, A.V., et al., *J. Struct. Chem.*, 2013, vol. 54, no. 3, p. 598.
14. Ivanov, A.V., Zinkin, S.A., Sergienko, V.I., et al., *Russ. J. Inorg. Chem.*, 2011, vol. 56, no. 3, p. 409.
15. Zaeva, A.S., Ivanov, A.V., Gerasimenko, A.V., and Sergienko, V.I., *Russ. J. Inorg. Chem.*, 2015, vol. 60, no. 2, p. 203.
16. Zaeva, A.S., Ivanov, A.V., and Gerasimenko, A.V., *Russ. J. Coord. Chem.*, 2015, vol. 41, no. 10, p. 644.
17. Ivanov, A.V., Bredyuk, O.A., Loseva, O.V., and Rodina, T.A., *Russ. J. Coord. Chem.*, 2015, vol. 41, no. 2, p. 108.
18. Ivanov, A.V., Bredyuk, O.A., Loseva, O.V., and Antzutkin, O.N., *Russ. J. Inorg. Chem.*, 2016, vol. 61, no. 6, p. 755.
19. Ivanov, A.V., Loseva, O.V., Rodina, T.A., et al., *Russ. J. Coord.Chem.*, 2016, vol. 42, no. 2, p. 104.
20. Cox, M.J. and Tiekink, E.R.T., *Z. Kristallogr.*, 1997, vol. 212, no. 7, p. 542.
21. Iwasaki, H., *Acta Crystallogr.*, *Sect. B*: *Struct. Crystallogr. Cryst. Chem.*, 1973, vol. 29, p. 2115.
22. Hexem, J.G., Frey, M.H., and Opella, S.J., *J. Chem. Phys.*, 1982, vol. 77, no. 7, p. 3847.
23. Harris, R.K., Jonsen, P., and Packer, K.J., *Magn. Reson. Chem.*, 1985, vol. 23, no. 7, p. 565.
24. Pines, A., Gibby, M.G., and Waugh, J.S., *J. Chem. Phys.*, 1972, vol. 56, no. 4, p. 1776.
25. *APEX2 (version 1.08), SAINT (version 7.03), SADABS (version 2.11) and SHELXTL (version 6.12),* Madison (WI, USA): Bruker AXS Inc., 2004.
26. Exarchos, G., Robinson, S.D., and Steed, J.W., *Polyhedron*, 2001, vol. 20, nos. 24–25, p. 2951.
27. Elwej, R., Hannachi, N., Chaabane, I., et al., *Inorg. Chim. Acta*, 2013, vol. 406, p. 10.
28. Pauling, L., *The Nature of the Chemical Bond and the Structure of Molecules and Crystals*, London: Cornell Univ., 1960.
29. Bondi, A., *J. Phys. Chem.*, 1964, vol. 68, no. 3, p. 441.
30. Bondi, A., *J. Phys. Chem.*, 1966, vol. 70, no. 9, p. 3006.
31. Alcock, N.W., *Adv. Inorg. Chem. Radiochem.*, 1972, vol. 15, no. 1, p. 1.
32. Lidin, R.A., Andreeva, L.L., and Molochko, V.A., *Spravochnik po neorganicheskoi khimii* (Handbook in Inorganic Chemistry), Moscow: Khimiya, 1987.

Translated by E. Yablonskaya